

Low Photon Number Non-Invasive Imaging Through Time-Varying Diffusers

Adrian Makowski^{1,2}, Wojciech Zwolinski¹, Pawel Szczypkowski¹,
Bernard Gorzkowski¹, Sylvain Gigan², Radek Lapkiewicz^{1,*}

¹Institute of Experimental Physics, Faculty of Physics, University of
Warsaw, Pasteura 5, 02-093 Warsaw, Poland.

²Laboratoire Kastler Brossel, École normale supérieure (ENS)–
Université Paris Sciences & Lettres (PSL), CNRS, Sorbonne Université,
Collège de France, 24 rue Lhomond, Paris, 75005, France.

*Corresponding author(s). E-mail(s): radek.lapkiewicz@fuw.edu.pl;
Contributing authors: adrian.makowski@fuw.edu.pl;
w.zwolinski2@student.uw.edu.pl; p.szczypkowski@student.uw.edu.pl;
bernard.gorzkowski@gmail.com; sylvain.gigan@lkb.ens.fr;

Abstract

Scattering poses a significant challenge in optical imaging. In microscopy, it leads to progressive degradation of image quality preventing sample examination at increasing depths. As the thickness of the sample increases, the number of photons that can successfully pass through it decreases, leading to a reduced signal and preventing us from obtaining clear images. Imaging becomes even more difficult with dynamic scatterers like biological tissues that change over time. We demonstrate non-invasive imaging of fluorescent objects hidden behind dynamic diffusers. Our reconstruction uses a stack of images recorded for different diffuser realizations and works even when individual camera frames contain small photon numbers.

Keywords: Imaging in dynamic complex media, Single photon detection, Non-invasive imaging, Speckle pattern analysis

1 Introduction

Scattering plays a crucial role in determining the appearance of observed objects. When scattering occurs multiple times within a medium, such as biological tissues, fog, or clouds, it is referred to as a complex medium. Light propagation through complex media results in random interference patterns known as speckle patterns[1]. For a long time, light scattering in complex media was considered uncontrollable. This fundamental challenge of light scattering affects not only imaging [2], but also poses obstacles in communication, spectroscopy, and other optical and photonic technologies.

Imaging through complex media has long been seen as a formidable challenge. However, a groundbreaking experiment by Vellekoop and Mosk [3] demonstrated that by controlling wavefronts through spatial light modulators (SLMs), light can be focused through scattering media. Subsequent experiments by Popoff et al. made significant advancements by introducing a method to measure the transmission matrix of complex media, allowing for wavefront control using SLMs behind these media [4, 5].

These remarkable advancements led to a better understanding of complex media and paved the way for developing non-invasive imaging techniques through such media. Specifically, experiments [6, 7] utilized the phenomenon known as the memory effect. Within small regions, when an input wavefront reaching a complex medium is tilted within a certain angular range, the output wavefront is equally tilted, resulting in the translation of the speckle pattern behind the complex medium [8, 9]. In imaging, within a memory effect region, light emitted from each point source behind the complex medium creates an almost identical speckle pattern that is shifted according to the position of the source origin.

Methods presented in [6, 7, 10] utilize the memory effect to reconstruct objects hidden behind complex media by calculating the spatial autocorrelation of speckle images and employing iterative phase retrieval algorithms. An alternative group of methods relies on fluctuating, random speckle illumination and observing the sample’s response [11, 12]. Some of these methods use Non-negative matrix factorization (NMF) to disentangle the temporal and spatial information about the sample [11, 13, 14]. More recently, well-established reflection-matrix techniques were applied to incoherent fluorescence imaging [12].

While several techniques for imaging in complex media were developed and represent significant achievements, their widespread adoption remains limited. One limitation is that these techniques typically work with static diffusers. In live bioimaging, biological tissues change over time, necessitating methods that can handle dynamic scattering. Similarly, LIDAR must operate in fog, which changes over time. Some approaches to overcome this issue involve using high-speed digital micromirror devices (DMDs) [15–19] as spatial light modulators (SLMs) for fast transmission matrix measurement. However, all these methods require high signal levels, which hinder their practical applications. For rapidly changing diffusers, one must acquire light over a short period, resulting in low light intensities being captured. This creates a growing need for robust imaging techniques that work in low-light scenarios through dynamic complex media.

Here, we demonstrate a non-invasive technique for imaging behind dynamic scattering layers. This technique is capable of operating in the low-photon regime and

with single photon cameras, with much less than one photon per pixel on average. We demonstrate our technique in a widefield fluorescence microscope to image astrocyte cells stained with the common dye Alexa Fluor 568 through a dynamically changing diffuser, recording less than one photon per camera pixel per frame. Our method does not require wavefront shaping, transmission matrix characterization, or light focusing through the complex medium.

2 Principles

Our method for imaging through a dynamic diffuser is based on techniques such as those presented in [6, 7, 10]. The method involves recording a movie of a luminescent object behind a changing diffuser (see Figure 1a). We assume that the frame duration is short enough for the diffuser to remain static during each frame. We demonstrate that our approach enables robust reconstruction even if individual frames do not have a sufficient detected photon number for object reconstruction.

When the medium changes during the integration time, the resulting speckle pattern blurs, leading to an averaged-out image that loses spatial information about the sample. To overcome this, rather than directly integrating the signal recorded by the camera, we divide the signal into short-exposure, low-photon frames. We compute the Fourier transform modulus for each frame and average the resulting matrices using root mean square. This method enables effective imaging in dynamic media, yielding improved results, particularly in low-light scenarios, compared to the techniques described by [6, 7, 10].

Since each frame I_i captured by the camera is a convolution of the object O with the speckle Point Spread Function (PSF) S_i of the varying diffuser (as illustrated in 1b), and the object is within the memory effect range [8, 9] (meaning each point of the object has the same PSF S_i), we have:

$$I_i = O * S_i,$$

where $i = 1, 2, 3, \dots, N$ is the frame index, and N is the total number of frames.

This implies that

$$\mathcal{F}\{I_i\} = \mathcal{F}\{O\}\mathcal{F}\{S_i\},$$

where $\mathcal{F}\{I_i\}$, $\mathcal{F}\{O\}$, and $\mathcal{F}\{S_i\}$ denote the spatial Fourier transforms of each frame I_i , the object O , and the speckle Point Spread Function S_i , respectively (as shown in 1c). Then,

$$\sqrt{\frac{1}{N} \sum_{i=1}^N |\mathcal{F}\{I_i\}|^2} = |\mathcal{F}\{O\}| \sqrt{\frac{1}{N} \sum_{i=1}^N |\mathcal{F}\{S_i\}|^2}.$$

For many realizations of the diffuser, the root mean square of the Fourier transform moduli of the frames for the object recorded through the diffuser converges to the modulus of the Fourier transform of the object image without scattering:

$$\sqrt{\frac{1}{N} \sum_{i=1}^N |\mathcal{F}\{S_i\}|^2} \rightarrow |\mathcal{F}\{P\}|,$$

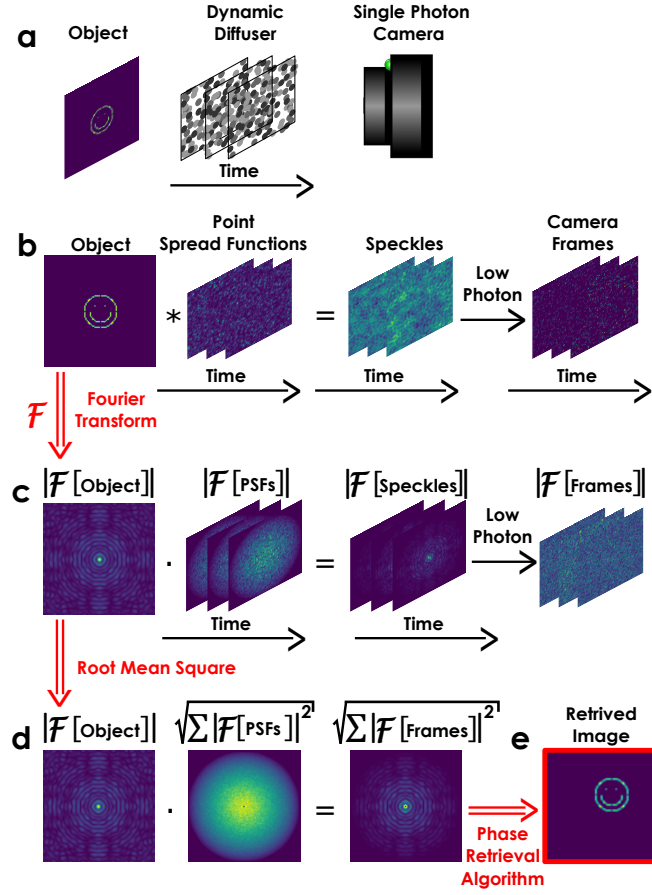


Fig. 1 Concept of our method. (a) Schematic of our experiment. We record a movie of a luminescent object behind a changing diffuser. Each frame is assumed to be captured fast enough to treat the diffuser as static during the exposure. (b) Each frame I_i is a convolution of the object O with the speckle PSF S_i of the varying diffuser. (c) The spatial Fourier transform of (b). (d) Averaging the Fourier transform moduli of all frames approximates the modulus of the Fourier transform of the object image without scattering. (e) The phase of the complex Fourier transform, lost in this process, is retrieved using a phase retrieval algorithm [20].

where $\mathcal{F}\{P\}$ denotes the spatial Fourier transform of the Point Spread Function not affected by the diffuser (as demonstrated in Figure 1d). Note that this is different from direct imaging, because the NA is defined by the combination of the scatterer and the objective [21].

As a result of this analysis, the only information lost is the complex phase of the Fourier transform of the object image without scattering. As demonstrated previously [6, 7, 10], this phase can be retrieved using a phase retrieval algorithm (like in Figure 1e). In our work, we utilized the combination of hybrid input-output (HIO) and the error-reduction (ER) algorithms [20].

In practice, we didn't directly average all the moduli of the Fourier transforms. Instead, we utilized several filtering techniques, such as removing the Gaussian envelope of the image and applying Hann windowing like in [7, 10]. For more details, please refer to the Methods section 5 and *Supplemental Material*.

3 Results

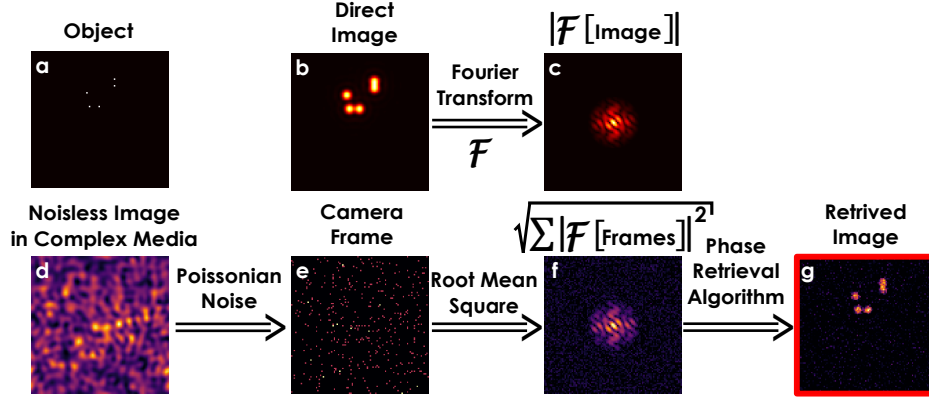


Fig. 2 Imaging in the photon counting regime – simulation results. (a) Original object. (b) Image of the object captured with a finite resolution imaging system. (c) Modulus of the Fourier transform of the object (b). (d) Image of the object obscured by the diffuser - a single frame captured by the camera. (e) Single camera frame with Poisson noise. (f) An average of Fourier transforms modulus of 10,000 frames. (g) Reconstructed object image through a dynamic diffuser.

To demonstrate the effectiveness of our method in the single photon counting regime, we first conducted a computer simulation. Figure 2 presents the simulation results of imaging the object through the dynamic diffuser in a low photon number regime. Figure 2a shows an object consisting of several point emitters. Imaging this object through an imaging system with finite resolution gives the image shown in Figure 2b ($I = O * PSF$), with the Fourier transform modulus shown in Figure 2c ($|\mathcal{F}\{I\}| = |\mathcal{F}\{O\}| |\mathcal{F}\{PSF\}|$).

Noiseless imaging of the object from Figure 2a through a diffuser results in the speckle image shown in Figure 2d ($I_i = O * S_i$). However, since each frame is short enough to capture the unchanged diffuser during its duration, the detected photon number is low. To account for this, we limit the number of photons detected during each frame from Figure 2d (adding a Poisson noise). Figure 2e shows a simulation of a single frame from Figure 2d with a limited number of photons.

In the simulation, we generated 10,000 frames, each with a different diffuser realization and an average of 400 photons per frame (0.04 photons per pixel). Figure 2f shows the root mean square of the Fourier transform moduli of these 10,000 frames ($\sqrt{\frac{1}{N} \sum_{i=1}^N |\mathcal{F}\{I_i\}|^2} = |\mathcal{F}\{O\}| \sqrt{\frac{1}{N} \sum_{i=1}^N |\mathcal{F}\{S_i\}|^2}$). Notably, Figure 2f closely

resembles Figure 2c. After applying the phase retrieval algorithm [20], we obtain the reconstructed image (Figure 2g), which closely resembles the direct image of the object in Figure 2b.

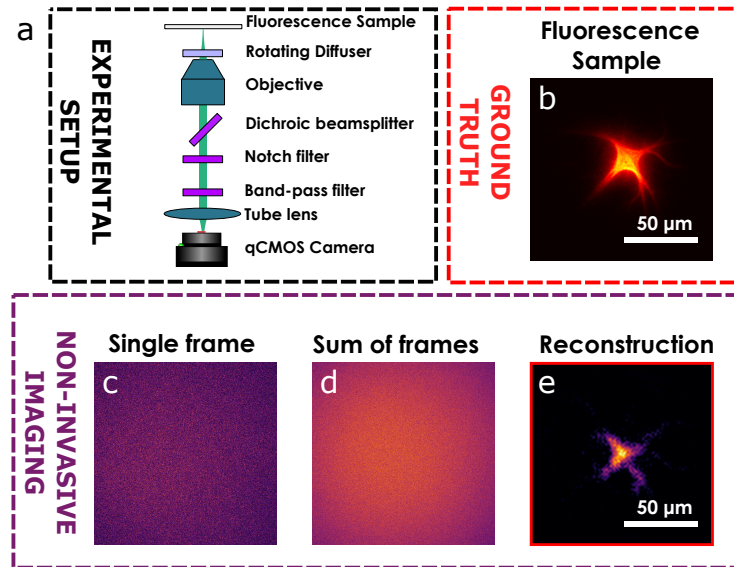


Fig. 3 Imaging of Alexa Fluor 568 stained astrocytes through the dynamic complex medium. (a) Schematic of the wide-field fluorescence microscope utilized in our experiments. (b) Direct image of the sample without the diffuser (ground truth). (c) Single frame captured by the qCMOS camera. (d) Average of all 1872 frames recorded. (e) Reconstruction result using the phase retrieval algorithm [20].

In our experiment, we applied our method to fluorescence microscopy. As an experimental setup, we utilized a wide-field custom-made microscope (see Figure 3a). The details of the microscope construction can be found in Section 5. Our microscope allowed for the insertion and removal of a dynamic diffuser, which was placed just before the microscope objective. As a sensor in our microscope, we used the Hamamatsu ORCA-Quest 2 qCMOS camera, which enables single photon counting. We demonstrated our experimental setup on a sample of astrocytes stained with the popular fluorescent dye Alexa Fluor 568. Details of the sample preparation procedure are provided in Methods section 5. Figure 3b shows a direct image of the sample without the diffuser. Figure 3c illustrates a single frame captured by the qCMOS camera. During a frame duration of 200.96 ms, we recorded an average of 1.85 photons per camera pixel. Figure 3d shows the root mean square of all 1872 frames recorded in our experiment. Figure 3d corresponds to the incoherent sums of all frames. Speckles are blurred out and don't exhibit any spatial information that could be retrieved. Therefore, we average the Fourier transform moduli of all the frames and apply a phase retrieval algorithm [20]. The reconstruction result using the phase retrieval algorithm [20] is presented in Figure 3e.

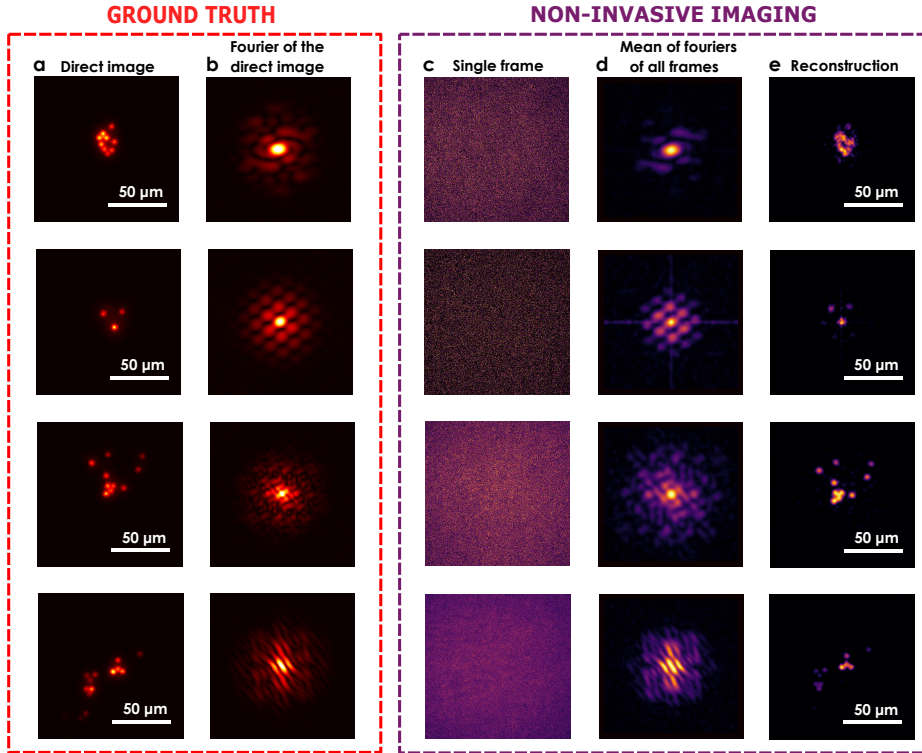


Fig. 4 Imaging of fluorescence micro-spheres through the dynamic complex medium. (a) Direct images of fluorescent microspheres without the diffuser. (b) The modulus of the Fourier transforms of the images in column (a). (c) The average of the Fourier transform moduli of the frames captured through the dynamic diffuser. (d) Recovered image computed using the phase retrieval algorithm [20].

To demonstrate the versatility of our method, we applied it to various objects constructed with fluorescent micro-spheres samples (see Figure 4). The sample preparation procedure for the micro-spheres is detailed in Section 5. The column **a** of Figure 4 shows direct images of the fluorescent micro-spheres in our microscope. Figure 4**b** presents the modulus of the Fourier transforms of the images in the column **a**. Figure 4**c** shows the average of the Fourier transform modulus of the frames captured by the camera through the dynamic diffuser. Figure 4**d** displays the recovered image imaged through the diffuser, computed using the column **c** from fig. 4 with the phase retrieval algorithm [20].

4 Discussion

We successfully demonstrated imaging through a dynamic diffuser at signal levels low enough to detect single photons. Our method, like techniques presented in [6, 7, 10], does not require physical alteration of the sample, nor does it necessitate characterizing

the medium’s transmission matrix or focusing light through it. However, our approach is specifically optimized for low-photon conditions and dynamic diffusers – a scenario highly relevant for deep tissue imaging. This approach can be implemented without adaptive optics or wavefront shaping systems.

We tested our method using a standard fluorescence microscope and applied it to various fluorescent samples. Notably, we successfully imaged astrocyte cells stained with the widely used dye Alexa Fluor 568, as well as various challenging objects constructed from fluorescent micro-spheres, further underscoring the versatility and effectiveness of our approach. Although we demonstrated our technique in microscopy, it has potential applications in various other fields of imaging. For instance, it can be utilized in LIDAR to cope with time-varying fog [22, 23], in astronomy for imaging distant, dim objects through a fluctuating atmosphere [24], and in endoscopy using multimode fibers [25, 26], where bends generate changing scattering scenarios.

Single camera frames in our experiment contain low signals, reaching 0.33 photons per pixel per frame (around 10^6 per frame). These experiments are feasible thanks to recent advances in the development of single photon cameras. The camera that we utilized has a relatively low frame rate, capturing fewer than 5 frames per second for the full field of view required by the speckle size. A potential improvement in the data acquisition rate our setup is the use of SPAD arrays, which are increasingly being applied in imaging [27–31]. Recent advancements in this field have led to the development of megapixel SPAD arrays [29], making their practical application in widefield microscopy feasible. Cameras based on SPAD technology allow for single photon detection with high temporal resolution, providing a powerful tool for enhancing various bioimaging techniques and other applications. In our application, orders of magnitude improvement of temporal resolution offered by SPAD arrays will enable imaging through extremely fast varying diffusers.

5 Methods

5.1 Experimental setup

We designed and constructed our experimental setup, which consisted of a fluorescence wide-field microscope. For the objective, we used Nikon S Plan Fluor ELWD 20x/0.45, and for the excitation beam, we utilized a Spectra-Physics Millennia PRO laser with a wavelength of 532 nm. We utilized several neutral density filters to attenuate the laser beam. The fluorescence sample was placed within the working distance of the primary objective, while a rotating diffuser (Edmund Holographic Diffuser of 5° Diffusing Angle) was positioned adjacent to the microscope objective. To select the desired field of view in our experiment, we illuminated the sample from a transmissive side using another objective (Nikon Nikon S Plan Fluor ELWD 40x/0.60), which was usually out of focus to provide a large excitation spot.

To filter the fluorescence light from the excitation source, we employed a dichroic mirror (Edmund 552), a long-pass filter (Thorlabs FELH0550), and a notch filter Semrock NF01-532U-25. Additionally, to ensure good visibility of speckles, a band-pass filter (Thorlabs FBH590-10) was used. The tube lens in our setup was a Thorlabs

TTL200-A with a focal length of 200 mm. The ORCA-Quest 2 qCMOS camera from Hamamatsu was positioned at the focal point of the tube lens.

Mounts for the fluorescence sample and the rotating diffuser with its motor were custom-designed and 3D-printed.

For more details of the experimental setup, please refer to Supplementary information.

5.2 Data acquisition

In our experiment, we utilized a galvo mirror (Thorlabs GVS211/M) positioned in the excitation laser beam path to modulate the illumination of the sample. The galvo mirror was connected to a microcontroller (Arduino Micro), which communicated with a computer via a serial port. A Python program controlled both the microcontroller and the camera.

Initially, the computer sent a command to the Arduino to illuminate the sample and then to the camera to begin capturing light. The microcontroller ensured that the fluorescent sample was illuminated only during the camera's light detection period to limit the photo-bleaching of the sample. It was removing the excitation laser beam immediately after the camera sent a trigger indicating the end of the frame, ensuring precise synchronization.

The microcontroller used in our experiment had an additional task: controlling the rotation of the diffuser. The microcontroller was connected to an electronic circuit (L2930) that enabled it to switch the 12V power supply required for motor (SKU GS06331-10) rotation on and off.

5.3 Data analysis

We performed several filtering techniques in our data processing to retrieve the object.

First, we divided by a 2D Gaussian function. The speckle image on the camera is not equally distributed across the sample, exhibiting a Gaussian envelope. By dividing by a 2D Gaussian function, we corrected for this uneven distribution.

Next, we applied a 2D Hann filter to smooth the edges of each frame, which helps mitigate edge effects in the Fourier domain.

After applying the Hann filter, we computed each frame's 2D Fourier transform and calculated its modulus. We then averaged with the root mean square these transformed frames and convolved the resulting signal with a narrow 2D filter to remove speckle artifacts.

Finally, we applied the phase retrieval algorithm (the combination of hybrid input-output (HIO) and the error-reduction (ER) algorithms) to the prepared Fourier amplitude, to obtain a reconstructed object.

5.4 Sample preparation

Fluorescence micro-spheres

Fluorescent microsphere samples were prepared using a drop-casting method. A concentrated solution of fluorescent microspheres (PS-FluoRed-Particles; 4.99

$\mu\text{m}/\text{SD}=0.16 \mu\text{m}$; 530/607 nm) was significantly diluted with ethanol. The solution was subjected to a 15-minute sonication bath to prevent the clustering of the fluorescent microspheres. A 50 μL drop of this diluted solution was then placed onto a microscope coverslip and allowed to air dry.

Alexa Fluor 568 stained astrocyte

Three-week-old primary mixed neuronal cultures on glass slides were fixed in PBS with 4% paraformaldehyde and 4% sucrose for 8 minutes at 37°C. After washing three times with PBS containing 4% sucrose, cells were permeabilized with 0.25% Triton X-100 for 2 minutes. Blocking was performed in PBS with 3% BSA and 0.1% Triton X-100 for 1 hour at room temperature. Cultures were incubated overnight at 4°C with an anti-GFAP primary antibody (1:1000, #ab7260), followed by three PBS washes. Secondary antibody incubation was conducted for 1 hour at room temperature using Alexa Fluor 568-conjugated anti-rabbit antibody (1:500, #A-11011). After three PBS washes, samples were mounted on glass slides using Fluoromount-G solution (#00-4958-02).

Acknowledgements. We would like to express our sincere gratitude to Diana Legutko for preparing the Alexa Fluor 568-stained astrocyte samples, and to Anat Daniel for insightful discussions and comments about the experimental setup. We also acknowledge the support of the following funding agencies: Narodowe Centrum Nauki (grants 2023/49/N/ST7/04195 and 2022/47/B/ST7/03465); Fundacja na rzecz Nauki Polskiej (FIRST TEAM project POIR.04.04.00-00-3004/17-00); the European Regional Development Fund (POIR.04.04.00-00-3004/17-00); HORIZON EUROPE Marie Skłodowska-Curie Actions (FLORIN ID 101086142); and the French Government Scholarship for Ph.D. Cotutelle/Codirection.

References

- [1] Goodman, J. W. *Speckle phenomena in optics: theory and applications* (Roberts and Company Publishers, 2007).
- [2] Yoon, S. *et al.* Deep optical imaging within complex scattering media. *Nature Reviews Physics* **2**, 141–158 (2020).
- [3] Vellekoop, I. M. & Mosk, A. P. Focusing coherent light through opaque strongly scattering media. *Opt. Lett.* **32**, 2309–2311 (2007).
- [4] Popoff, S., Lerosey, G., Fink, M., Boccarda, A. C. & Gigan, S. Image transmission through an opaque material. *Nature communications* **1**, 81 (2010).
- [5] Popoff, S. M. *et al.* Measuring the transmission matrix in optics: An approach to the study and control of light propagation in disordered media. *Physical review letters* **104**, 100601 (2010).

- [6] Bertolotti, J. *et al.* Non-invasive imaging through opaque scattering layers. *Nature* **491**, 232–234 (2012).
- [7] Katz, O., Heidmann, P., Fink, M. & Gigan, S. Non-invasive single-shot imaging through scattering layers and around corners via speckle correlations. *Nature photonics* **8**, 784–790 (2014).
- [8] Freund, I., Rosenbluh, M. & Feng, S. Memory effects in propagation of optical waves through disordered media. *Physical review letters* **61**, 2328 (1988).
- [9] Judkewitz, B., Horstmeyer, R., Vellekoop, I. M., Papadopoulos, I. N. & Yang, C. Translation correlations in anisotropically scattering media. *Nature physics* **11**, 684–689 (2015).
- [10] Hofer, M., Soeller, C., Brasselet, S. & Bertolotti, J. Wide field fluorescence epimicroscopy behind a scattering medium enabled by speckle correlations. *Optics express* **26**, 9866–9881 (2018).
- [11] Zhu, L. *et al.* Large field-of-view non-invasive imaging through scattering layers using fluctuating random illumination. *Nature communications* **13**, 1447 (2022).
- [12] Weinberg, G., Sunray, E. & Katz, O. Noninvasive megapixel fluorescence microscopy through scattering layers by a virtual reflection-matrix. *arXiv preprint arXiv:2312.16065* (2023).
- [13] Moretti, C. & Gigan, S. Readout of fluorescence functional signals through highly scattering tissue. *Nature Photonics* **14**, 361–364 (2020).
- [14] Rimoli, C. V. *et al.* Demixing fluorescence time traces transmitted by multimode fibers. *Nature Communications* **15**, 6286 (2024).
- [15] Conkey, D. B., Caravaca-Aguirre, A. M. & Piestun, R. High-speed scattering medium characterization with application to focusing light through turbid media. *Optics express* **20**, 1733–1740 (2012).
- [16] Conkey, D. B., Brown, A. N., Caravaca-Aguirre, A. M. & Piestun, R. Genetic algorithm optimization for focusing through turbid media in noisy environments. *Optics express* **20**, 4840–4849 (2012).
- [17] Goorden, S. A., Bertolotti, J. & Mosk, A. P. Superpixel-based spatial amplitude and phase modulation using a digital micromirror device. *Optics express* **22**, 17999–18009 (2014).
- [18] Mitchell, K. J., Turtaev, S., Padgett, M. J., Čížmár, T. & Phillips, D. B. High-speed spatial control of the intensity, phase and polarisation of vector beams using a digital micro-mirror device. *Optics express* **24**, 29269–29282 (2016).

- [19] Hellman, B. & Takashima, Y. Angular and spatial light modulation by single digital micromirror device for multi-image output and nearly-doubled étendue. *Optics Express* **27**, 21477–21496 (2019).
- [20] Fienup, J. R. Phase retrieval algorithms: a comparison. *Appl. Opt.* **21**, 2758–2769 (1982).
- [21] Mosk, A. Exploiting disorder for perfect focusing. *Nature photonics* **4**, 320–322 (2010).
- [22] Miclea, R.-C., Dughir, C., Alexa, F., Sandru, F. & Silea, I. Laser and lidar in a system for visibility distance estimation in fog conditions. *Sensors* **20**, 6322 (2020).
- [23] Bijelic, M., Gruber, T. & Ritter, W. A benchmark for lidar sensors in fog: Is detection breaking down? *2018 IEEE intelligent vehicles symposium (IV)* 760–767 (2018).
- [24] Tyson, R. K. & Frazier, B. W. *Principles of adaptive optics* (CRC press, 2022).
- [25] Čižmár, T. & Dholakia, K. Exploiting multimode waveguides for pure fibre-based imaging. *Nature communications* **3**, 1027 (2012).
- [26] Plöschner, M., Tyc, T. & Čižmár, T. Seeing through chaos in multimode fibres. *Nature photonics* **9**, 529–535 (2015).
- [27] Lubin, G. *et al.* Quantum correlation measurement with single photon avalanche diode arrays. *Opt. Express* **27**, 32863–32882 (2019).
- [28] Ghezzi, A. *et al.* Multispectral compressive fluorescence lifetime imaging microscopy with a spad array detector. *Optics letters* **46**, 1353–1356 (2021).
- [29] Bruschini, C., Homulle, H., Antolovic, I. M., Burri, S. & Charbon, E. Single-photon avalanche diode imagers in biophotonics: review and outlook. *Light: Science & Applications* **8**, 87 (2019).
- [30] Slenders, E. *et al.* Confocal-based fluorescence fluctuation spectroscopy with a spad array detector. *Light: Science & Applications* **10**, 31 (2021).
- [31] Lukashchuk, A. *et al.* Photonic-electronic integrated circuit-based coherent lidar engine. *Nature Communications* **15**, 3134 (2024).

Supplementary information - Low Photon Number Non-Invasive Imaging Through Time-Varying Diffusers

Adrian Makowski^{1,2}, Wojciech Zwolinski¹, Pawel Szczypkowski¹,
Bernard Gorzkowski¹, Sylvain Gigan², Radek Lapkiewicz^{1,*}

¹Institute of Experimental Physics, Faculty of Physics, University of
Warsaw, Pasteura 5, 02-093 Warsaw, Poland.

²Laboratoire Kastler Brossel, École normale supérieure (ENS)–
Université Paris Sciences & Lettres (PSL), CNRS, Sorbonne Université,
Collège de France, 24 rue Lhomond, Paris, 75005, France.

*Corresponding author(s). E-mail(s): radek.lapkiewicz@fuw.edu.pl;
Contributing authors: adrian.makowski@fuw.edu.pl;
w.zwolinski2@student.uw.edu.pl; p.szczypkowski@student.uw.edu.pl;
bernard.gorzkowski@gmail.com; sylvain.gigan@lkb.ens.fr;

Abstract

This Supplementary Material adds more details to the main manuscript in the four sections. Section 1 explains the experimental setup, describing the equipment and methods used. Section 2 presents a theoretical investigation regarding our method. Section 3 covers the data analysis process, showing how we handled the data. Finally, Section 4 presents the simulation results, helping to support and explain our experimental findings.

Keywords: Imaging in dynamic complex media, Single-photon detection,
Non-invasive imaging, Speckle pattern analysis

1 Experimental setup

For the experimental validation of our concept, we constructed a custom microscope setup. It was designed for stability during long experiments, flexibility, and simplicity.

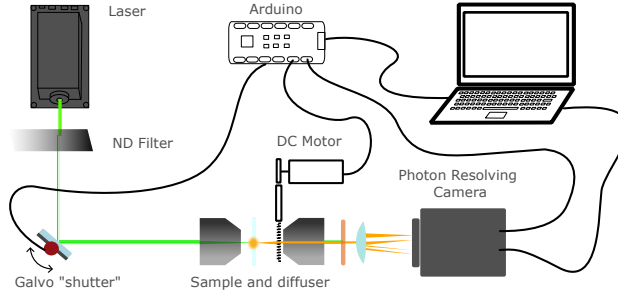


Fig. 1 Schematic of the experimental setup: The 532 nm excitation laser reflects off the galvo mirror, which acts as a shutter. During acquisition, the galvo mirror directs the light into the objective, illuminating the desired area on the fluorescent sample (beads or astrocytes). The fluorescence passes through a diffuser, which is rotated by a random angle during acquisitions. A second objective collects the scattered fluorescent light. The fluorescence is then separated from the remaining pump light using spectral filters. Finally, it is imaged onto a photon-resolving camera via a tube lens. Acquisition and illumination are synchronized using an Arduino board.

As the excitation source, we used a Spectra-Physics Millennia PRO laser with a wavelength of 532 nm. The laser was attenuated using a reflective neutral density filter (Thorlabs ND30A) and a gradient ND filter (Thorlabs NDL-10C-4). The beam was then directed by a galvanometric mirror (Thorlabs GVS011/M). This mirror acted as a shutter, directing the pump light to the rest of the setup only during camera exposure (“ON-state”). This reduced the bleaching of fluorophores during long experiments.

The 532 nm light passed through the objective on the transmissive side (Nikon S Plan Fluor ELWD 40x/0.60). The distance of the objective to the sample determined the illumination area. Green light excited the fluorescent beads or Alexa Fluor 568-stained astrocyte cultures. The resulting fluorescence propagated to a diffuser (Edmund Holographic Diffuser with a 5° diffusing angle). The diffuser was housed in a 3D-printed enclosure that allowed it to rotate freely. It was coupled to a DC motor with a set of gears. A slight loosening of the parts increased the randomization of the diffuser placement. The diffuser was positioned close to a second objective (Nikon S Plan Fluor ELWD 20x/0.45), which collected the scattered fluorescent light. The collected fluorescence passed through a dichroic mirror (Thorlabs DMLP550R). This mirror reflected most of the pump light. Residual 532 nm light was filtered using a notch filter (Semrock NF01-532U-25) and a bandpass filter (Thorlabs FBH590-10). The fluorescence was collected with a tube lens (Thorlabs TTL200-A). This lens projected the speckle pattern onto a QCMOS sensor (Hamamatsu Orca Quest). Data collection was managed by a computer connected to an Arduino board.

The Arduino was used to synchronize the camera, galvo mirror, and rotating diffuser. For each frame, a command was sent to the Arduino to switch on the DC motor for a random duration (0 to 0.5 seconds). After rotation, the galvo mirror was set to “ON-state,” and the camera exposure was triggered. The exposure time was read from the camera’s output electrical lines. Once the exposure ended, the galvo mirror was turned to “OFF-state.” Frames were collected using Python code with Micro-Manager for easy camera access.

For our experiments, we collected 1000 to 10000 frames. The photon-resolving mode of the camera allowed for short exposures (up to 1 μs). However, it required long readout times (around 200 ms per frame). This extended the duration of a single measurement to several hours.

2 Theoretical investigation

2.1 Low photon regime

We can estimate a lower bound for the power that has to be produced by the fluorescent dyes if we want to achieve at least two photons per frame with the following considerations:

- The duration of a frame must be much shorter than the characteristic time of change of the scattering medium:

$$t_{frame} \ll t_{scatt}$$

- The energy arriving on the camera during a frame is at least the energy of two photons:

$$2E_{photon} < E_{camera}$$

$$2\frac{hc}{\lambda} < P_{camera}t_{frame}$$

(λ is the wavelength emitted by the dye, P_{camera} the power received by the camera).

- Photons emitted by the fluorescent dyes arrive to the camera only if they are emitted within the solid angle given by the numerical aperture (assuming no scatterer):

$$P_{camera} = \frac{\Omega}{4\pi} P_{fluo} = \frac{NA^2}{4} P_{fluo}$$

We arrive at the following inequality for the total power emitted by the fluorescent dyes:

$$P_{fluo} \gg \frac{8hc}{NA^2\lambda t_{scatt}}$$

Given this inequality and the properties of the dyes used in a given setup, if the characteristic time of the dynamic scattering medium is known, one can estimate the theoretical minimum laser power required to apply our method.

3 Data analysis

Our data analysis follows the methodologies presented in [1–3], but adapted for the single-photon regime. All data analysis and simulations were conducted using Python with standard libraries such as NumPy, Torch, and SciPy.

3.1 Removal of Gaussian envelope

In our data processing, we employed several filtering techniques to retrieve the Fourier amplitude of the object. One of the key steps was correcting for the uneven brightness distribution caused by vignetting in our imaging system, which manifests as reduced brightness at the edges of the image compared to the center. We addressed this by dividing each frame by a 2D Gaussian function that models the intensity envelope.

To compute the Gaussian correction, we employed a Fourier-based approach using Python. First, the Fourier transform of each frame was computed using a 2D Fast Fourier Transform (FFT). A mask, with a size determined by `Gaussian_filter_length`, was applied in the Fourier domain to isolate the central portion of the spectrum corresponding to the Gaussian envelope. The inverse FFT was then performed to obtain the spatial-domain Gaussian, which was subsequently used to normalize the original frame by dividing the image intensity by the Gaussian envelope.

Here is a simplified representation of the process in Python:

```
A_FL = np.fft.fftshift(np.fft.fft2(I)) # Perform FFT and shift
NN1, NN2 = np.shape(I) # Get the shape of the image
T = np.zeros((NN1, NN2)) # Create an empty mask
# Apply Gaussian filter to the central part of the spectrum
T[(NN1//2)-Gaussian_filter_length+1:(NN1//2)+Gaussian_filter_length+1,
  (NN2//2)-Gaussian_filter_length+1:(NN2//2)+Gaussian_filter_length+1
 ] = 2
A_FL = A_FL * T # Multiply the FFT by the mask
A_FL = np.abs(np.fft.ifft2(A_FL)) # Inverse FFT
#to get the Gaussian envelope
I_New = I[:, :] / A_FL[:, :] # Normalize the image by the Gaussian
```

3.2 Hann filtering

In our image processing, the edges of each frame can introduce artifacts, especially when applying Fourier transforms. These edge effects arise because the Fourier transform assumes the image is periodic. If there are sudden discontinuities at the image boundaries, this assumption is violated, leading to unwanted high-frequency components, in the Fourier domain. Such artifacts degrade the quality of the reconstructed image and must be mitigated for accurate analysis.

To address this issue, we applied a two-dimensional (2D) Hann filter to the frames, which smooths the edges by gradually tapering pixel intensities towards zero near the boundaries. The Hann window is a tapering function that prevents sharp intensity transitions at the edges, ensuring smooth transitions and reducing artifacts caused by edge discontinuities.

The Hann window is defined as follows:

$$w(n) = 0.5 \left(1 + \cos \left(\frac{2\pi n}{N-1} \right) \right)$$

where n is the pixel index and N is the total number of pixels in a given image dimension. By multiplying the image by the Hann window along both the x and y axes, we ensure that the pixel intensity tapers smoothly towards zero at the edges.

The following Python code demonstrates the application of the 2D Hann filter:

```
# Smoothing of image edges with Hann windowing
hann_x = hann(I_New.shape[0]) # Create Hann window for x-dimension
hann_y = hann(I_New.shape[1]) # Create Hann window for y-dimension
hann_window = np.outer(hann_x, hann_y) # Generate 2D Hann window
I_New = I_New * hann_window # Apply Hann window to the image
```

This filtering process reduces the sharp edge discontinuities in the frames, minimizing high-frequency artifacts and producing cleaner results when applying the Fourier transform.

3.3 Fourier modulus estimation

After applying the Hann filter to reduce high-frequency noise, we computed the 2D Fourier transform of each frame and calculated its modulus. The mean square of these transformed frames was then computed, and the resulting signal was convolved with a narrow 2D Gaussian filter to mitigate speckle artifacts.

It is important to note that the diffuser used in our setup has finite dimensions. This results in a limited number of diffuser realizations, meaning that the relationship:

$$\frac{1}{N} \sum_{i=1}^N |\mathcal{F}\{S_i\}|^2 \neq |\mathcal{F}\{P\}|^2$$

where S_i represents the speckle point spread function (PSF) of the i -th frame, and P is the PSF without a diffuser. This inequality indicates that the summation of the Fourier transform moduli over multiple frames does not fully converge to the PSF of the undisturbed object, primarily due to the limited number of diffuser realizations. Consequently, residual artifacts from the diffuser may persist in the reconstructed image.

To mitigate these residual artifacts, we convolve the resulting signal with a narrow 2D Gaussian filter, which effectively removes speckle effects without significantly altering the squared Fourier modulus of the object, as the object typically lacks the high frequencies present in the speckles.

Finally, we subtract the background from the processed 2D array and calculate the square root to recover the Fourier transform modulus of the object.

3.4 Phase retrieval algorithm

Finally, we applied a phase retrieval algorithm to the prepared Fourier amplitude, utilizing the combination of hybrid input-output (HIO) and the error-reduction (ER) algorithm [4]. This allowed us to reconstruct the object.

The phase retrieval process was implemented using the following Python code. The function below runs multiple trials of the phase retrieval process with various settings, including the use of a GPU for acceleration:

```
def run_PR(Fixed_Amp, Ptrial=10, Method='HIO', iterations=30, beta_max=3,
```

```

beta_min=0.8, Beta_step=-0.01, useGPU=False):
    ReconstructionResultStore = []

    for k in range(Ptrial):
        if Method == 'HIO':
            print('HIO Method')
            Reconstruct_Field, recons_err, recons_err2
            = HIO_BasicPhaseRetrieval(
                np.fft.ifftshift(Fixed_Amp), beta_max, Beta_step,
                beta_min, iterations,
                np.random.rand(np.shape(Fixed_Amp)[0],
                               np.shape(Fixed_Amp)[1]), useGPU)

            Reconstruct_Image_Amp = np.abs(Reconstruct_Field)
            plt.imshow(Reconstruct_Image_Amp)
            plt.colorbar()
            plt.show()

            ReconstructionResultStore.append(Reconstruct_Image_Amp)
            print(f'End of No. {k} trial\n\n')

    return ReconstructionResultStore
def HIO_BasicPhaseRetrieval(sautocorr_temp, beta_start, beta_step,
beta_stop, N_iter, init_guess, useGPU=False):
    if useGPU:
        sautocorr = torch.from_numpy(sautocorr_temp).cuda()
        g1 = torch.from_numpy(init_guess).cuda()

    BETAS = torch.arange(beta_start, beta_stop-beta_step, beta_step)
    with torch.no_grad():
        for beta in BETAS:
            for _ in range(N_iter):
                G_uv = torch.fft.fft2(g1)
                g1_tag = torch.real(torch.fft.ifft2(sautocorr * G_uv
                / torch.abs(G_uv)))
                g1 = g1_tag * ((g1_tag >= 0).int())
                + ((g1_tag < 0).int())
                * (g1 - beta * g1_tag)

            for _ in range(N_iter):
                G_uv = torch.fft.fft2(g1)
                g1_tag = torch.real(torch.fft.ifft2(sautocorr * G_uv
                / torch.abs(G_uv)))
                g1 = g1_tag * ((g1_tag >= 0).int())

```

```

recons_err = torch.mean(torch.mean(
(torch.abs(torch.fft.fft2(g1)) - sautocorr) ** 2))
recons_err2 = torch.sqrt(torch.mean(torch.mean(
(torch.abs(torch.fft.fft2(g1)) ** 2 - sautocorr ** 2) ** 2)))

g1 = g1.cpu().numpy()
recons_err = recons_err.cpu().numpy()
recons_err2 = recons_err2.cpu().numpy()
else:
    sautocorr = sautocorr_temp
    g1 = init_guess

    BETAS = np.arange(beta_start, beta_stop - beta_step,
beta_step)
    for beta in BETAS:
        for _ in range(N_iter):
            G_uv = np.fft.fft2(g1)
            g1_tag = np.real(np.fft.ifft2(sautocorr
* G_uv / np.abs(G_uv)))
            g1 = g1_tag * (g1_tag >= 0).astype(int)
            + (g1_tag < 0).astype(int)
            * (g1 - beta * g1_tag)

recons_err = np.mean(np.mean((np.abs(np.fft.fft2(g1))
- sautocorr) ** 2))
recons_err2 = np.sqrt(np.mean(np.mean(
(np.abs(np.fft.fft2(g1)) ** 2 - sautocorr ** 2) ** 2)))

return [g1, recons_err, recons_err2]

```

4 Simulations

4.1 Photon Distribution Across Various Frame Number

We simulated a constant number of photons, distributing them across varying numbers of camera frames. Each frame was simulated with a different realization of the diffuser. For each frame, we calculated the modulus of the Fourier transform, summed these moduli, and then compared the result to the Fourier transform modulus of a direct image without a diffuser, taken with a large number of photons. To quantitatively assess the difference between the two Fourier transform results, we normalized both matrices using the Frobenius norm, subtracted one from the other, and calculated the Frobenius norm of the resulting difference matrix:

$$\text{Error} = \left\| \frac{F_{\text{sum}}}{\|F_{\text{sum}}\|_F} - \frac{F_{\text{direct}}}{\|F_{\text{direct}}\|_F} \right\|_F$$

where F_{sum} is the Fourier transform modulus of the summed frames and F_{direct} is the Fourier transform modulus of the direct image. Identical matrices would result in a norm value of 0, indicating perfect similarity.

The simulation results, shown in Figure 2, compare the error values for 2, 4, 6, 8, and 10 million photons. The X-axis represents the number of frames, while the Y-axis indicates the corresponding error values.

The results reveal an optimal number of frames over which the photons should be distributed for each given photon number.

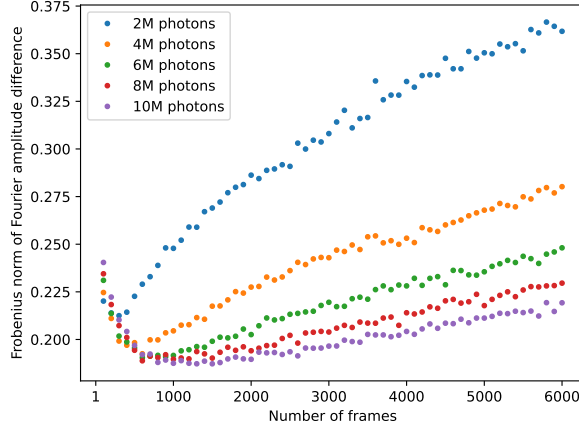


Fig. 2 The impact of distributing a constant number of photons across varying frame numbers on the accuracy of the reconstructed image. This analysis illustrates a comparison of simulation results for different photon numbers (2, 4, 6, 8, and 10 million). The X-axis represents the number of frames used in the simulations, while the Y-axis shows the corresponding error values.

5 Simulation with Limited Diffuser Realizations

In this simulation, we maintained a constant number of camera frames while limiting the number of possible diffuser realizations. Similar to the previous section, we calculated the modulus of the Fourier transform for each frame, summed these moduli, and compared the result to the Fourier transform modulus of a direct image obtained without a diffuser, using a large number of photons. The comparison was again quantified using the error metric:

$$\text{Error} = \left\| \frac{F_{\text{sum}}}{\|F_{\text{sum}}\|_F} - \frac{F_{\text{direct}}}{\|F_{\text{direct}}\|_F} \right\|_F$$

Figure 3 presents the results of this simulation, comparing the outcomes for 4, 8, 12, 16, and 20 million photons. The X-axis represents the number of diffuser realizations, while the Y-axis displays the corresponding error values.

The results indicate that increasing the number of diffuser realizations improves the accuracy of estimating the object's Fourier moduli.

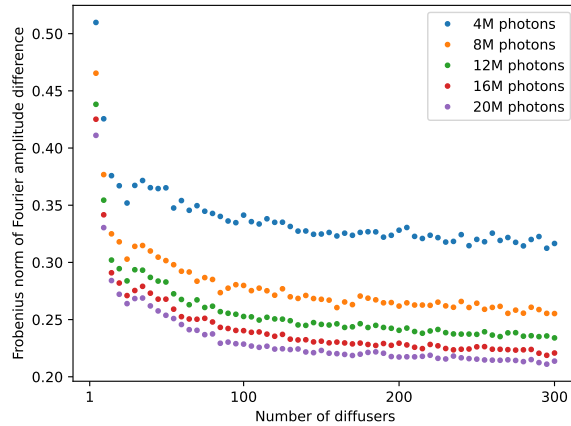


Fig. 3 Comparison of simulation results with a limited number of diffuser realizations for different photon counts numbers (4, 8, 12, 16, and 20 million). The X-axis represents the number of diffuser realizations, while the Y-axis shows the corresponding error values.

References

- [1] Bertolotti, J. *et al.* Non-invasive imaging through opaque scattering layers. *Nature* **491**, 232–234 (2012).
- [2] Katz, O., Heidmann, P., Fink, M. & Gigan, S. Non-invasive single-shot imaging through scattering layers and around corners via speckle correlations. *Nature photonics* **8**, 784–790 (2014).
- [3] Hofer, M., Soeller, C., Brasselet, S. & Bertolotti, J. Wide field fluorescence epi-microscopy behind a scattering medium enabled by speckle correlations. *Optics express* **26**, 9866–9881 (2018).
- [4] Fienup, J. R. Phase retrieval algorithms: a comparison. *Appl. Opt.* **21**, 2758–2769 (1982).